ITC 1/54
Information Technology and Control
Vol. 54 / No. 1/ 2025
pp. 147-163
DOI 10.5755/j01.itc.54.1.39833

Driver Fatigue Detection Based on Multiple Physiological Signals and an Improved Deep Belief Network

Received 2024/12/16 | Accepted after revision 2024/02/12

HOW TO CITE: Wang, L., Liu, Y., Yin, X., Li, J., Gu, Y. (2025). Driver Fatigue Detection Based on Multiple Physiological Signals and an Improved Deep Belief Network. *Information Technology and Control*, 54(1), 147-163. https://doi.org/10.5755/j01.itc.54.1.39833

Driver Fatigue Detection Based on Multiple Physiological Signals and an Improved Deep Belief Networks

Lin Wang, Yuxuan Liu, Xiaowei Yin, Jiaqi Li, and Yulin Gu

Department of Mechanical Engineering, Shenyang Institute of Engineering, Shenyang, 110136 China;

wanglin@sie.edu.cn (L. W.), l932817947@sohu.com (Y. L.), yinxw@sie.edu.cn (X. Y.), lijiaqi9846@163.com (J. L.), yulingu8@gmail.com (Y. G.)

Lin Wang and Xiaowei Yin contribute the same to the article and are the corresponding authors.

Corresponding author: wanglin@sie.edu.cn (L. Wang), yinxw@sie.edu.cn (X.W. Yin)

In order to accurately discriminate the driver fatigue, multiple physiological signals of 10 drivers were collected by a wireless body area network in actual driving, including neck electromyography (EMG) and electroencephalography (EEG). Then, the noises of signals were removed by several denoising methods, including ICEEMDAN (improved complete ensemble empirical mode decomposition with adaptive noise), WT (wavelet threshold denoising), and ICEEMDAN-WT. 22 features, including time domain features (e.g., variance and mean square root), frequency domain features (e.g., average power spectral density and frequency centre), and nonlinear features (e.g., energy entropy, information entropy and multiscale entropy) were extracted, including energy entropy, multiscale entropy, and other relevant features. Subsequently, a deep belief network (DBN) was used to further extract multi-domain features. And then, a grey wolf optimization algorithm was used to optimize the performance of the DBN. The results showed that the accuracy of the model built in the present work was up to 96% in discriminating the fatigue states.

KEYWORDS: Driver fatigue; EMG signal; EEG signal; Feature parameters; Deep belief network.

1. Introduction

Driver fatigue is a predominant factor contributing to traffic accidents, accounting for 43% of major incidents [2, 11], and poses a serious threat to the safety of individuals. Consequently, accurately discriminating the fatigue level of drivers to ensure optimal road traffic safety is highly practical. Currently, detection methods for driver fatigue primarily include behavioural observation [17, 9], vehicle control performance evaluation [3], and physiological indices monitoring. Behavioural observation involves collecting facial expression and body posture information through sensors such as monitors. Vehicle control performance evaluation relies on onboard sensors and computer models to analyse indicators such as reaction time and braking response. These two approaches have achieved notable technological advancements. Physiological signals are unaffected by subjective consciousness and are considered the most precise method for driver fatigue detection at the present [4, 5, 10, 15, 16, 19-21, 25]. Wang et al. [23] verified that cervical lumbar electromyography (EMG) signals can serve as key information in discriminating driver fatigue levels. The feasibility of assessing drivers' mental fatigue based on functional connectivity was validated through electroencephalography (EEG) analysis [6]. The original physiological signals collected by sensors often contain a substantial amount of noise from multiple sources, necessitating denoising process. Xi et al. [26] used the empirical mode decomposition (EMD) algorithm for noise reduction in physiological signal processing and achieved promising outcomes. Additionally, Jin et al. [13] applied wavelet denoising to electrocardiogram (ECG) data, enhancing the accuracy of driver fatigue detection based on ECG signals. Machine learning has been widely used in the field of classification discrimination. In a study conducted by Reference [27], a support vector machine (SVM) was used for the discrimination of driver fatigue based on physiological signals. However, traditional machine learning algorithms rely heavily on manual feature extraction and struggle to process longer data signals. References [14, 29] used a convolutional neural network (CNN) for training multimodal physiological signals. But CNNs are primarily designed for processing two-dimensional data. References [28, 18] demonstrated the effectiveness of the deep belief network (DBN) in extracting features from physiological signals.

Based on above literatures review, in the real-time driver fatigue detection field, the selection of signals, denoising methods, and classification methods are still challenges [1, 24]. The details include, (1) comprehensive analyses of the effects of multiple physiological signals and their combinations are lacking, leading to inconsistent conclusions. (2) Traditional denoising algorithms for physiological signals often encounter issues such as modal aliasing that adversely affect signal quality. (3) Deep neural networks require setting numerous hyperparameters for classification and discrimination tasks, and determining scientifically and reasonably hyperparameters is urgently needed to enhance the efficiency and accuracy of neural network.

Therefore, driver fatigue detection in real driving was investigated in the present work. The main research contents and originalities are, (1) Multiple physiological signals, including EEG and EMG, were collected from drivers during real driving experiments. (2) A denoising method of combining improved complete ensemble empirical mode decomposition with adaptive noise (ICEEMDAN) and wavelet thresholding was proposed to solve the problem of potential pseudo modes during signal decomposition. (3) A deep learning model based on the DBN was established to accurately evaluate the fatigue status of motor vehicle drivers. (4) The grey wolf algorithm was used to optimize the DBN parameters to improve the training efficiency and model accuracy.

2. Experimental Methods

The experiments involved 10 healthy volunteers (male, 22-35 years old, 60-85 kg, and more than two years of driving experience) continuously driving for 120 minutes on the Shenyang to Dandong section of the Danfu Expressway, maintaining a controlled speed not exceeding 100 km/h. It is well known, during driving, neck muscle fatigue and mental fa-

Figure 1
Diagram of a real driving experiment: (a) Experimental design for real driving experiments; (b) Schematic diagram of electrode placement positions

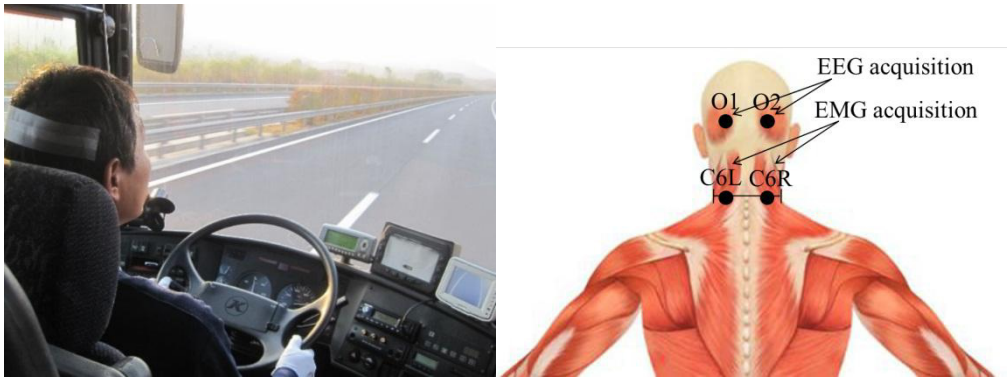

(a) (b)

tigue may cause the drowsiness, lack of concentration, and slow response. These are the predominant factors contributing to traffic accidents. Therefore, the neck electromyography (EMG) and the electroencephalography (EEG) are most sensitive for driver fatigue, and then they are selected as the signals to real-time evaluate driver fatigue. The experimental design and electrode placement positions for physiological signal collection are shown in Figure 1. Physiological signals were recorded by a portable wearable device for the participants, and the sampling frequency is 200 Hz. The data were received through a wireless body area network, and the collected data were sent directly to the processing system. Moreover, throughout the driving experiments, in order not to disturb the normal driving of the drivers, auxiliary personnel aided the drivers in completing the Swedish Occupational Fatigue Inventory-25 (SOFI-25) subjective questionnaire every 15 minutes. This questionnaire assesses five aspects of drivers' experience: lack of energy, exhaustion, physical discomfort, lack of motivation, and drowsiness. Each aspect is rated on a scale from 0 to 10, with higher scores indicating stronger feelings. The table represents participants' subjective evaluation of their current level of fatigue based on personal experience and assists in determining whether the driver has reached a state of fatigue.

3. Algorithm Principle

3.1. Denoising Algorithm Principle

3.1.1. ICEEMDAN

The ICEEMDAN algorithm proposed by Colomina [7] in 2014 addresses the issue of residual noise and pseudo mode that arise when processing signals using algorithms such as EMD and CEEMDAN. ICEEMDAN exhibits superior robustness and scalability, thereby enabling its application in scenarios with stringent requirements on noise robustness and scalability. In this paper, the ICEEMDAN algorithm was applied to preliminarily denoise physiological signals following the steps outlined in [12].

1. Define the operator E_k as the kth intrinsic mode function (*IMF*) component through the EMD of a signal.
2. Define the operator M as the local mean of the signal.
3. Using EMD to decompose the original sequence signal x iteratively I times. First, according to Equations (1)-(2), the first-order residual r_1 and the first-order IMF_1 are calculated. Similarly, according to Equations (3)-(4), the k^{th}-order residual r_k and the k^{th}-order IMF_k are calculated.

$$r_1 = 1/I\sum_{i=1}^{I} M(x+\varepsilon_0\omega^{(i)}[n]) \quad (1)$$

$$IMF_1 = x - r_1 \quad (2)$$

$$r_k = 1/I\sum_{i=1}^{I} M[r_{k-1}+\varepsilon_{k-1}E_k(\omega^{(i)})] \quad (3)$$

$$IMF_k = r_{k-1} - r_k \quad (4)$$

In Equation (1) and Equation (3), $\omega^{(i)}$ is the i^{th} group of Gaussian white noise added. In each round of the *IMF* calculation, the added noise signal is the *IMF* component of the original noise signal. ε_j is the coefficient multiplied by the noise component and represents the ratio of the signal-to-noise ratio of the added noise to the standard deviation of the noise component. The number of white noise group and ε_j are the input parameters of the ICEEMDAN algorithm.

4 The final residual R and the original sequence signal x are calculated as follows,

$$R = x - \sum_{k=1}^{k} IMF_k \quad (5)$$

$$x = R + \sum_{k=1}^{k} IMF_k \quad (6)$$

3.1.2. Wavelet Threshold Denoising

The wavelet threshold denoising method is an algorithm based on the multiresolution analysis of wavelet transforms. Because the wavelet decomposition coefficients of the noise signal and the useful signal in different frequency bands have different intensity distributions, the wavelet coefficients corresponding to the noise in each frequency band can be removed, and the wavelet decomposition coefficients of the original signal can be retained. Then, the processed coefficients are reconstructed by the wavelet, and the signal with relatively less noise can be obtained.

The steps of wavelet threshold denoising are as follows [8]:

1 Select the appropriate wavelet function, which requires good adaptability to nonstationary signals, good information compression and good retention of the original information.

2 According to the statistical characteristics of the signal, select an appropriate threshold criterion.

3 Carry out the inverse transform of wavelet coefficients after threshold processing to obtain the processed signal.

The criterion expression of wavelet threshold denoising is as follows,

$$\hat{W}_{j,k} = \begin{cases} sign(\omega_{j,k})(|\omega_{j,k}| - \lambda), & |\omega_{j,k}| \le \lambda \\ 0, & |\omega_{j,k}| \ge \lambda \end{cases} \quad (7)$$

In Equation (7), $\hat{W}_{j,k}$ is the wavelet transform coefficient after denoising, ω_j, k is the wavelet transform coefficient before denoising, and the "*sign*" is a sign function.

3.1.3. ICEEMDAN-WT

In this paper, the method of combining the ICEEMDAN algorithm with wavelet threshold (WT) denoising is proposed for signal denoising. First, the ICEEMDAN algorithm is used to decompose the signal into multiple IMF components, and then, some IMF components are retained according to the Spearman correlation coefficient method. Finally, the wavelet threshold denoising algorithm is used to filter out the high-frequency noise with low energy from the retained IMF component, after which the final denoised signal is reconstructed. Also, this method can avoid the disturbances caused by road conditions when extracting signal features.

3.2. Model Establishment

3.2.1. DBN Principle

A DBN is usually composed of several restricted Boltzmann machines (RBMs). Each RBM contains a visible layer and a hidden layer. The visible layer receives the input data and generates the corresponding hidden layer feature representation. The RBM structure is shown in Figure 2.

$v = (v_1, v_2, \cdots, v_n)$ represents the vector of the current state of the neurons in the visible layer, and $h = (h_1, h_2, \cdots, h_n)$ represents the vector of the current state of the neurons in the hidden layer. The energy function of the RBM is defined as:

$$E(v,h;\theta) = -\sum_{i=1}^{n} a_i v_i - \sum_{j=1}^{m} b_i h_i - \sum_{i=1}^{n}\sum_{j=1}^{m} \omega_{ij} v_i h_j \quad (8)$$

In Equation (8), a and b are the biases of the visible unit and the hidden unit in the RBM, respectively, ω_{ij}

Figure 2
Restricted Boltzmann machine

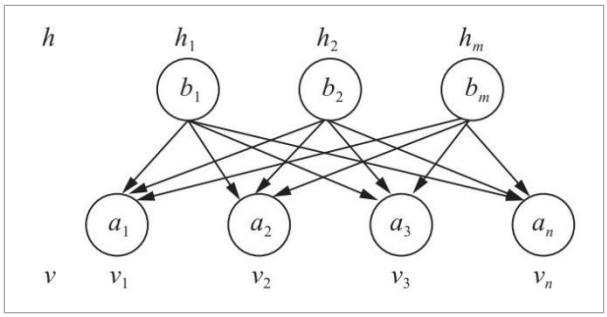

is the weight value between the two connected nodes, and $\theta = \{w, a, b\}$ is a parameter.

The node joint probability of the two layers of the model can be calculated by Equation (9):

$$P(v,h;\theta) = 1/Z(\theta)\exp(-E(v,h\,|\,\theta)) \tag{9}$$

In Equation (9), Z is the partition function, which represents the sum of all the neurons.

$$Z(\theta) = \sum_{v,h}\exp(-E(v,h\,|\,\theta)) \tag{10}$$

The conditional probability of the visual layer is shown in Equation (11):

$$P(v\,|\,h;\theta) = P(v,h;\theta)/P(h;\theta) = \prod_i P(v_i\,|\,h;\theta) \tag{11}$$

The hidden layer conditional probability is shown in Equation (12):

$$P(h\,|\,v;\theta) = P(v,h;\theta)/P(h;\theta) = \prod_j P(v_j\,|\,v;\theta) \tag{12}$$

The neurons between the same nodes are independent of each other, and the probability that the layer nodes are activated according to Equation (13):

$$P(v_i = 1\,|\,h;\theta) = 1/1+\exp(-a_i - \sum_{j=1}^{m}\omega_j h_j) \tag{13}$$

The probability of the hidden layer nodes being activated can be calculated according to Equation (14):

$$P(h_j = 1\,|\,v;\theta) = 1/1+\exp(-b_i - \sum_{j=1}^{m}\omega_j v_j) \tag{14}$$

Because the samples do not affect each other, the solution of the maximum likelihood function can be used to find the appropriate parameters. The likelihood function is shown in Equation (15):

$$L(\theta) = \prod_v L(\theta\,|\,v) = \prod_v P(v) \tag{15}$$

$$\partial \ln P(v)/\partial(\theta) = EP(h\,|\,v)\left[-\partial E(v,h)/\partial\theta\right] - \\ - EP(v,h)\left[-\partial E(v,h)/\partial\theta\right] \tag{16}$$

In Equation (15) and Equation (16), θ is the parameter in the RBM, and $E(v,h)$ is the energy function.

Then, all the parameter update criteria can be calculated according to Equation (17):

$$\begin{cases} \Delta\omega_{ij} = \varepsilon\left(v_i h_j P(h|v) - v_i h_j\right) \\ \Delta a_i = \varepsilon\left(v_i P(h|v) - v_i\right) \\ \Delta b_i = \varepsilon(h_i P(h\,|\,v) - h_i) \end{cases} \tag{17}$$

The hidden layer of each RBM is trained as the input of the next RBM. When all the RBM training is completed, the RBMs are initialized into a multilayer neural network. After backpropagation, the weights of the neural network parameters are fine-tuned. Finally, the softmax function is used to find the most likely corresponding label for each sample, thereby achieving effective classification. The final DBN model is shown in Figure 3.

Figure 3
Schematic diagram of the deep belief network (DBN) structure

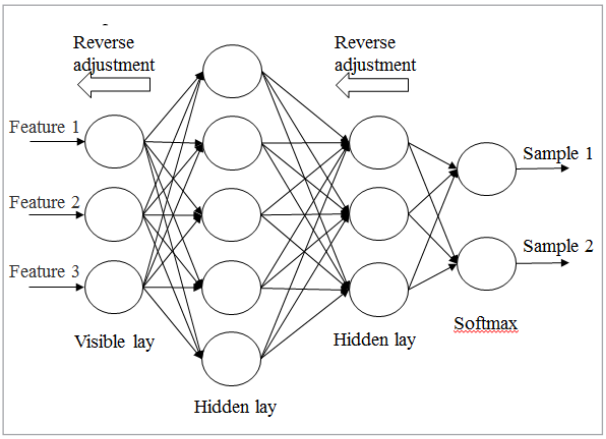

3.2.2. Grey Wolf Optimization Algorithm

The grey wolf optimizer (GWO) is a swarm intelligence algorithm based on the social behaviour of grey wolves in nature and is used to solve parameter optimization problems. The design inspiration of the GWO comes from the family structure and predation behaviour of grey wolf packs. In GWO, a certain number of grey wolves are randomly initialized. These grey wolves are sorted according to the size of the fitness function, and the searching-following-killing strategy is used to update the position according to certain rules. The grey wolf social hierarchy is shown in Figure 4. The principle of the algorithm is as follows.

Figure 4
Social hierarchy of grey wolves

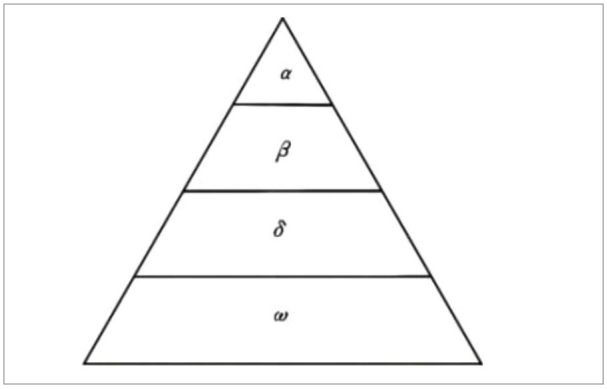

The first layer α of the pyramid is the leader in the population. The second layer of β is second only to α. The third layer of the pyramid δ carries out commands from α and β. The process of guiding other wolves to continue searching for the target is equivalent to finding a better solution for the model parameters. The remaining wolves ω are defined as candidate solutions whose positions are updated around α, β, and δ.

As a deep neural network model constructed by using multiple unsupervised learning algorithm layers, a DBN contains many parameters. Setting appropriate parameters can improve the network performance. In this paper, the grey wolf optimization algorithm is used to optimize the three important parameters of the DBN, the number of layers, the prelearning rate and the reverse adjustment learning rate.

Assuming that the population size of the grey wolf is N and that the search space has D dimensions, each dimension corresponds to a parameter to be optimized; thus, D=3 in this paper. The position of the i^{th} grey wolf in space can be expressed as

$$\overrightarrow{X_i} = \left(X_i^1, X_i^2, X_i^3\right),\ i = 1, 2, \cdots, N. \tag{18}$$

The position parameter of the grey wolf group is updated by Equation (19):

$$\overrightarrow{X}_i(t+1) = \overrightarrow{X}_p(t) - \vec{A} \cdot \left|\vec{C} \cdot \overrightarrow{X}_p(t) - \overrightarrow{X}(t)\right| \tag{19}$$

In Equation (19), t is the current number of iterations. $\overrightarrow{X}_p = \left(X_p^1, X_p^2, X_p^3\right)$ is the current prey position (optimal solution), $\vec{A} \cdot \left|\vec{C} \cdot \overrightarrow{X}_p(t) - \overrightarrow{X}(t)\right|$ is the size of the encircling step, and $\vec{A}$ and $\vec{C}$ are the coefficients, which can be defined as follows:

$$\vec{A} = 2\vec{a} \cdot \vec{r}_1 - \vec{a} \tag{20}$$

$$\vec{C} = 2 \cdot \vec{r}_2, \tag{21}$$

where the moduli of $\vec{r}_1$ and $\vec{r}_2$ are random numbers between [0, 1], $\vec{a}$ is the distance control parameter, and α decreases linearly from 2 as the number of iterations increases:

$$\alpha = 2 - 2t/t_{max}, \tag{22}$$

where $t_{\max}$ is the maximum number of iterations.

In Equation (23), $\overrightarrow{X}_\alpha(t+1)$, $\overrightarrow{X}_\beta(t+1)$, and $\overrightarrow{X}_\delta(t+1)$ are the updated position parameters α, β, and δ respectively, $\overrightarrow{X}(t)$ is the current position parameter of the other grey wolves. In Equation (24), $\overrightarrow{X}_\omega(t+1)$ is the final position of ω.

$$\begin{cases} \overrightarrow{X}_\alpha(t+1) = \overrightarrow{X}_\alpha(t) - \vec{A} \cdot \left|\vec{C} \cdot \overrightarrow{X}_\alpha(t) - \overrightarrow{X}(t)\right| \\ \overrightarrow{X}_\beta(t+1) = \overrightarrow{X}_\beta(t) - \vec{A} \cdot \left|\vec{C} \cdot \overrightarrow{X}_\beta(t) - \overrightarrow{X}(t)\right| \\ \overrightarrow{X}_\delta(t+1) = \overrightarrow{X}_\delta(t) - \vec{A} \cdot \left|\vec{C} \cdot \overrightarrow{X}_\delta(t) - \overrightarrow{X}(t)\right| \end{cases} \tag{23}$$

$$\overrightarrow{X}_\omega(t+1) = \left[\overrightarrow{X}_\alpha(t+1) + \overrightarrow{X}_\beta(t+1) + \overrightarrow{X}_\delta(t+1)\right]/3 \tag{24}$$

The wolves possess the capability to discern the initial location of prey (the optimal solution); however, within an abstract search space, the wolves encoun-

ter challenges in determining the exact position of prey. Therefore, in each iteration of the initial parameters (as in Equation (22)), the three current optimal solutions (α, β, and δ) obtained according to the goal of highest accuracy are saved, and other wolves are forced to update their positions according to Equation (23). The above steps should be repeated $t_{\max}$ times to ensure that the wolves are continuously approaching the target. Finally, the position parameter value of wolf α is the optimal solution for the number of DBN layers, prelearning rate and backwards adjustment learning rate of the established model.

4. Denoising Results

The original physiological signal of Figure 5 is decomposed by ICEEMDAN, and several IMF components are obtained, as shown in Figure 6.

Figure 5
A typical original physiological signal

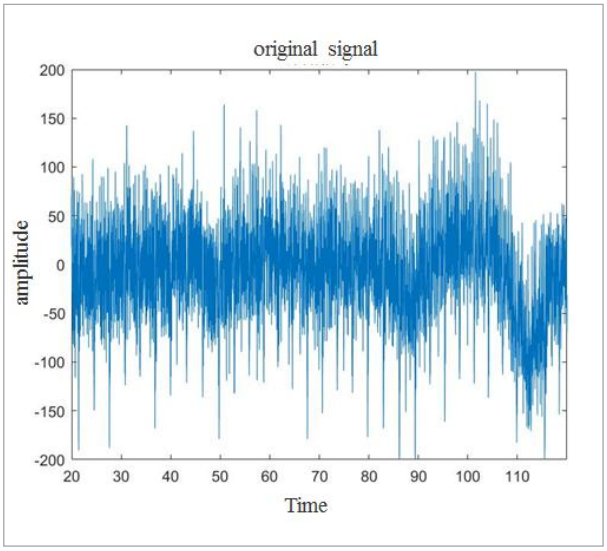

Figure 6
Decomposition diagram of ICEEMDAN

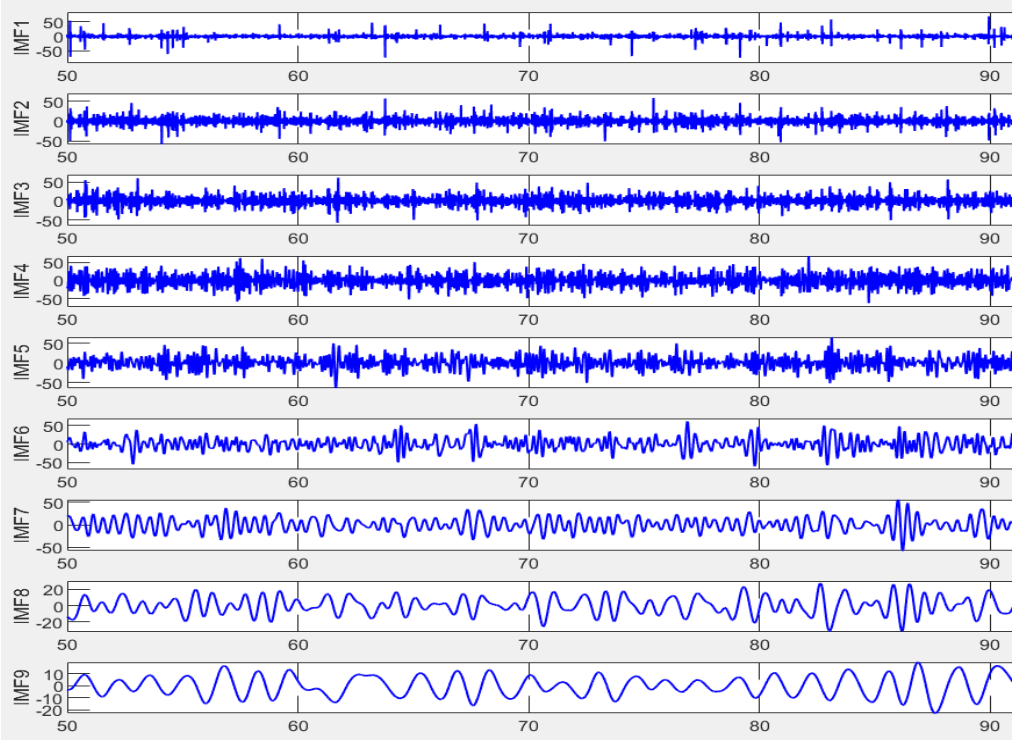

The fast Fourier transform of these components can be used to obtain the distribution of each component in the frequency domain, as shown in Figure 7.

Figure 7
Frequency domain distribution of the IMF

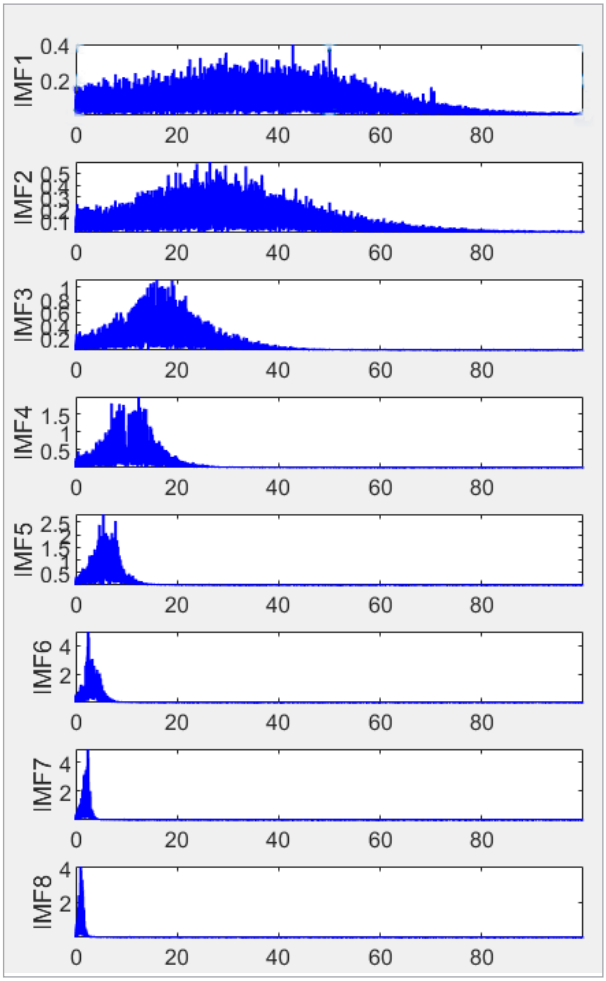

In this paper, an algorithm that combines ICEEMDAN and a wavelet threshold is used to denoise multimodal physiological signals. First, the original signal is decomposed into several parts using ICEEMDAN. The ratio of the standard deviation of ICEEMDAN noise to the information is set at 0.16. The average number of iterations is 50, and the maximum number of iterations is 200. The IMF component with a correlation coefficient greater than 0.3 to the original signal based on Spearman's autocorrelation coefficient method is retained. Then, the Symlet wavelet is select as the wavelet function, and three-layer wavelet decomposition is used to denoise the retained IMF component. Finally, the denoised IMF component via wavelet is reconstructed, and the final denoised signal can be obtained (shown in Figure 8).

Figure 8
A typical result of ICEEMDAN-WT denoising

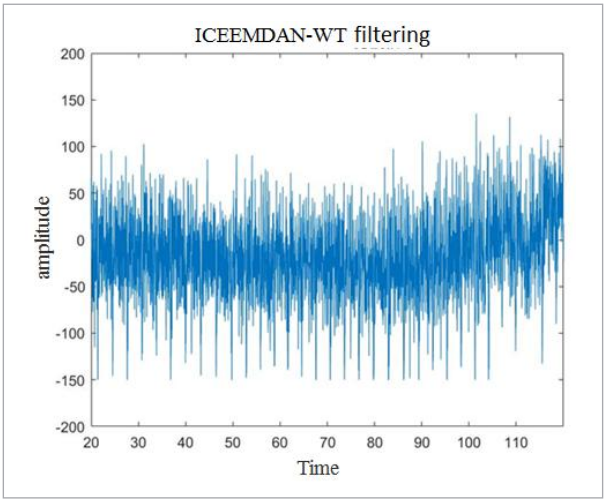

To demonstrate the superiority of our proposed denoising method, we compare it with only using wavelets for denoising (Figure 9). EMG signals are chosen here as an example. The waveform denoising effect using only wavelets is not significant, and large fluctuations still occur after denoising; however, after

Figure 9
A typical result of wavelet threshold denoising

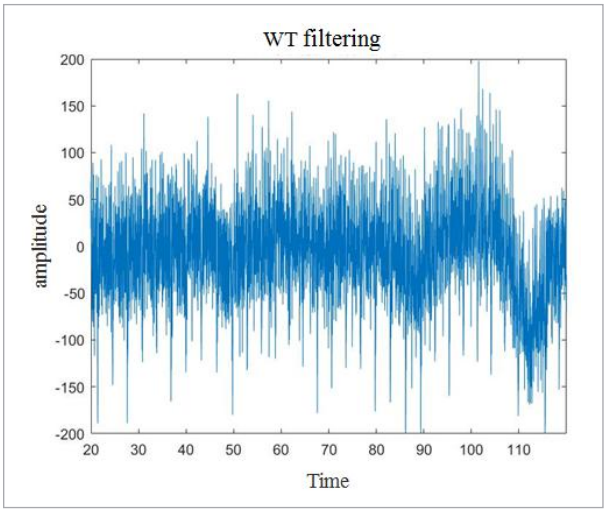

being processed by ICEEMDAN-WT, the waveform is significantly smoother because some low-frequency noise components are removed through correlation coefficients during ICEEMDAN, while high-frequency noise in signals is eliminated via wavelet thresholding; thus, combining both methods achieve excellent results.

5. Discrimination of Driver Fatigue Model

5.1. Model Establishment

The results of SOFI-25 are presented in Table 1. As driving time increases, the participants' scores on the subjective questionnaire exhibit an upwards trend, indicating a continuous increase in fatigue levels. Scores for the 0-30 min interval were close to zero, suggesting no fatigue among drivers during this period; however, the mean scores for the 90-120 min interval exceed six, indicating significant fatigue. Therefore, based on a combination of SOFI-25 and literatures review [22, 23], we propose the following definitions: state 1 corresponds to an "awake state" observed during the initial 0-30 min of the driving experiment, while state 2 represents a "fatigue state" experienced between 90-120 min.

To enhance both the accuracy and real-time performance of our fatigue discrimination model while reducing the data complexity, labelled feature vectors from drivers' original physiological signal dataset encompassing time domain features (e.g., variance and mean square root), frequency domain features (e.g., average power spectral density and frequency centre), and nonlinear features (e.g., energy entropy, information entropy and multiscale entropy) are initially extracted. Subsequently, these extracted labelled feature vectors are input into the DBN to further extract deep features that effectively represent the original information. This approach can reduce the computational complexity and achieve an accurate identification of drivers' fatigue states.

5.2. Construction of the Driver Fatigue Discrimination Model

The dataset is divided into a training set and a test set a ratio of 8:2 and randomly input into the DBN for training. The complete training flow chart of the driving fatigue discrimination model is shown in Figure 10.

In this paper, the grey wolf optimization algorithm is used to optimize the three important parameters of the DBN layer of Boltzmann machine, the prelearning rate, and the reverse adjustment learning rate. The whole optimal solution can be obtained as three DBN layers, a prelearning rate of 0.007, and a reverse adjustment learning rate of 2.0. To prove the effectiveness of the grey wolf optimization algorithm in optimizing the parameters, models with different parameters are constructed to compare the training process and results.

Under the condition of the same prelearning rate and reverse adjustment learning rate, DBN models composed of 2-layer, 3-layer, 4-layer and 5-layer RBMs

Table 1

Mean subjective questionnaire scores of participants at different times

Time/min	Part. 1	Part. 2	Part. 3	Part. 4	Part. 5	Part. 6	Part. 7	Part. 8	Part. 9	Part. 10	Ave.
0	0.0	0.0	0.0	0.0	0.0	0.0	0.0	0.0	0.0	0.0	0.0
15	0.0	0.0	0.0	0.0	0.0	0.0	0.0	0.0	0.0	0.0	0.0
30	0.6	0.8	0.2	0.4	0.6	0.2	0.4	0.6	0.8	0.0	0.5
45	1.8	1.8	2.4	2.2	1.8	2.6	2.5	2.6	2.6	2.6	2.1
60	3.6	4.2	4.4	3.4	3.4	3.8	3.8	3.6	4.0	3.8	3.8
75	5.4	6.2	5.2	5.6	6.8	5.2	6.4	5.0	5.4	4.8	5.7
90	6.2	7.0	6.8	5.8	7.0	5.6	7.0	6.6	6.8	5.8	6.4
105	6.8	7.6	7.6	6.4	7.8	6.2	8.0	7.2	7.4	6.8	7.2
120	7.8	8.0	8.0	7.6	8.0	7.0	9.0	8.4	8.6	7.8	8.0

Figure 10
Complete training process of the driver fatigue discrimination model

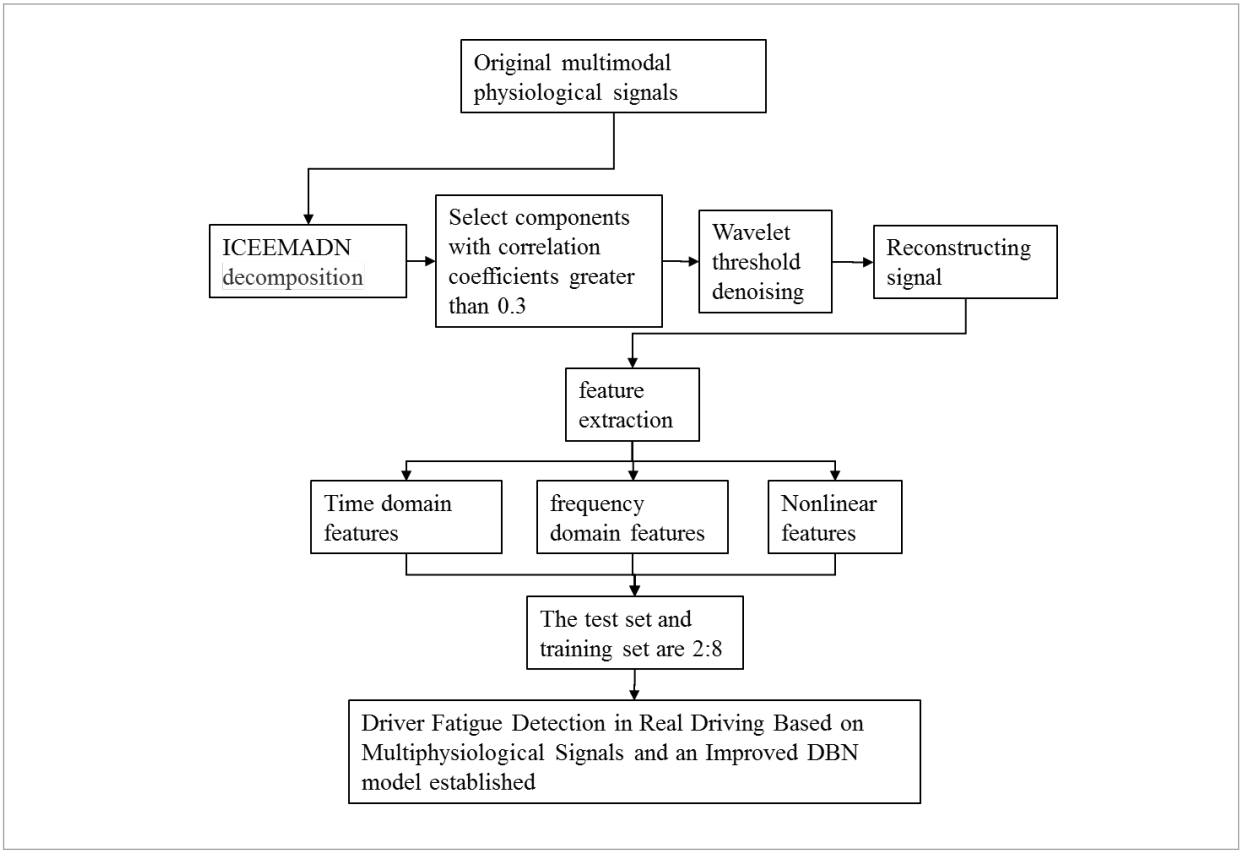

are constructed respectively, and the training results are shown in Figure 11. Under the condition of the same number of RBM layers and reverse adjustment learning rate, DBN models with prelearning rates of 0.003, 0.005, 0.007 and 0.009 are constructed respectively. The training results are shown in Figure 12. Under the condition of the same number of RBM layers and preadjusted learning rate, DBN models with reverse adjustment learning rates of 1.5, 2.0, 2.5 and 3.0 are constructed respectively. The training results are shown in Figure 13.

According to the above results, it can be concluded that the DBN parameters obtained by the grey wolf optimization algorithm proposed in this paper lead to higher accuracy and robustness than those of the other parameters. The specific parameters of the DBN are shown in Table 2.

The accuracy and loss function of the training process are shown in Figure 14, and the confusion matrix of the model is calculated and shown in Figure 15. State 1 corresponds to the nonfatigue state, while state 2 corresponds to the fatigue state. The comprehensive discrimination accuracy of the classification results of the fatigue discrimination model used in this paper reaches 96.67%, and the discrimination accuracy of the fatigue state reaches 100%, which indicates that the model proposed in this paper achieves a particularly high discrimination accuracy.

To further validate the reliability of the proposed model in this study, we sequentially input physiologi-

Figure 11

Effect of different layers of the DBN on the training process, with a prelearning rate of 0.007 and a reverse adjustment learning rate of 2.0: (a) Training process and results of a 3-layer Boltzmann machine; (b) Training process and results of the 2-layer Boltzmann machine; (c) Training process and results of a 4-layer Boltzmann machine; (d) Training process and results of a 5-layer Boltzmann machine

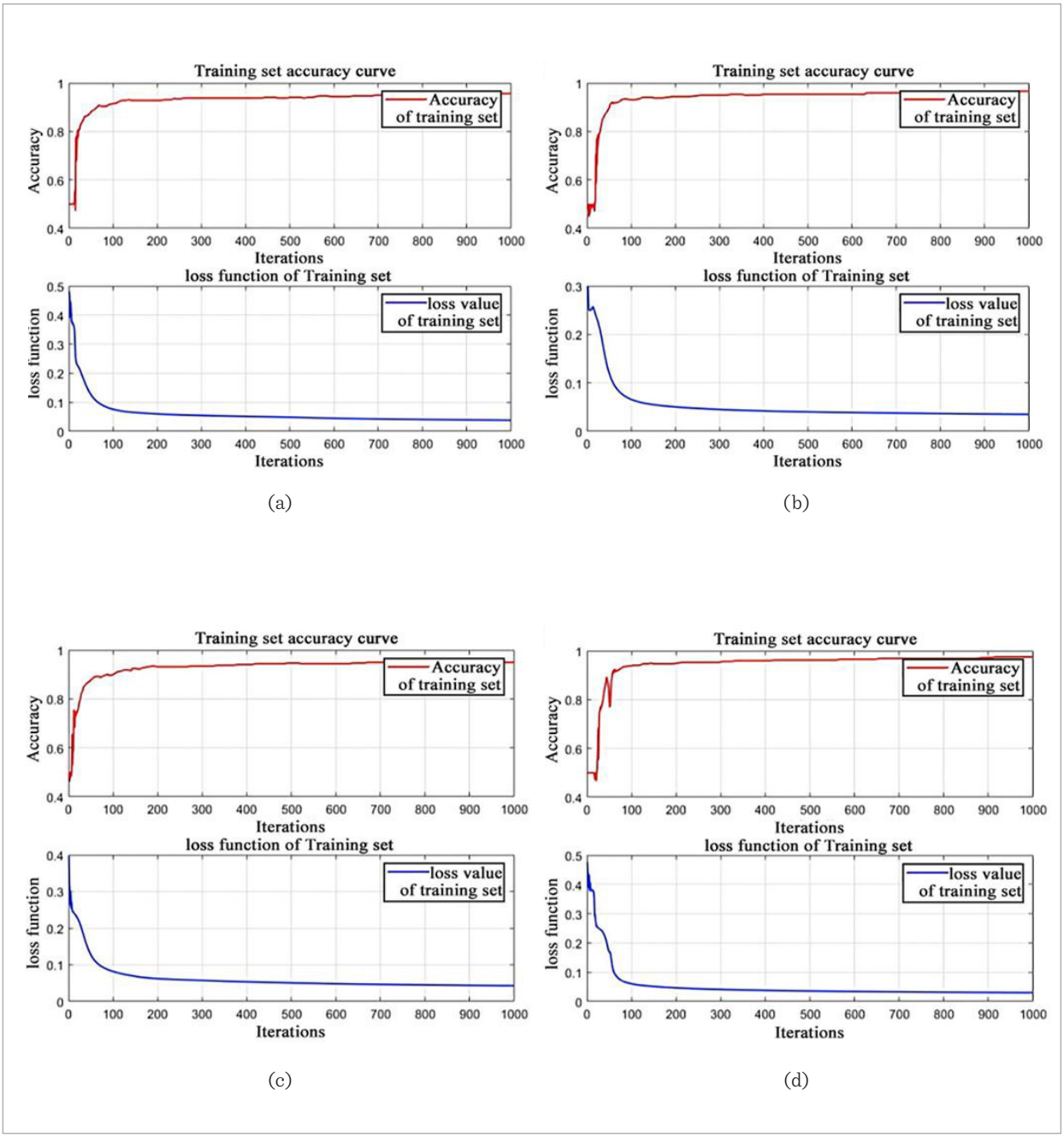

Figure 12

Effect of different prelearning rates on the training process of the DBN with a 3-layer of Boltzmann machine and a reverse adjusted learning rate of 2.0: (a) Training process and results with a prelearning rate of 0.007; (b) Training process and results with a prelearning rate of 0.003; (c) Training process and results with a prelearning rate of 0.005; (d) Training process and results with a prelearning rate of 0.009

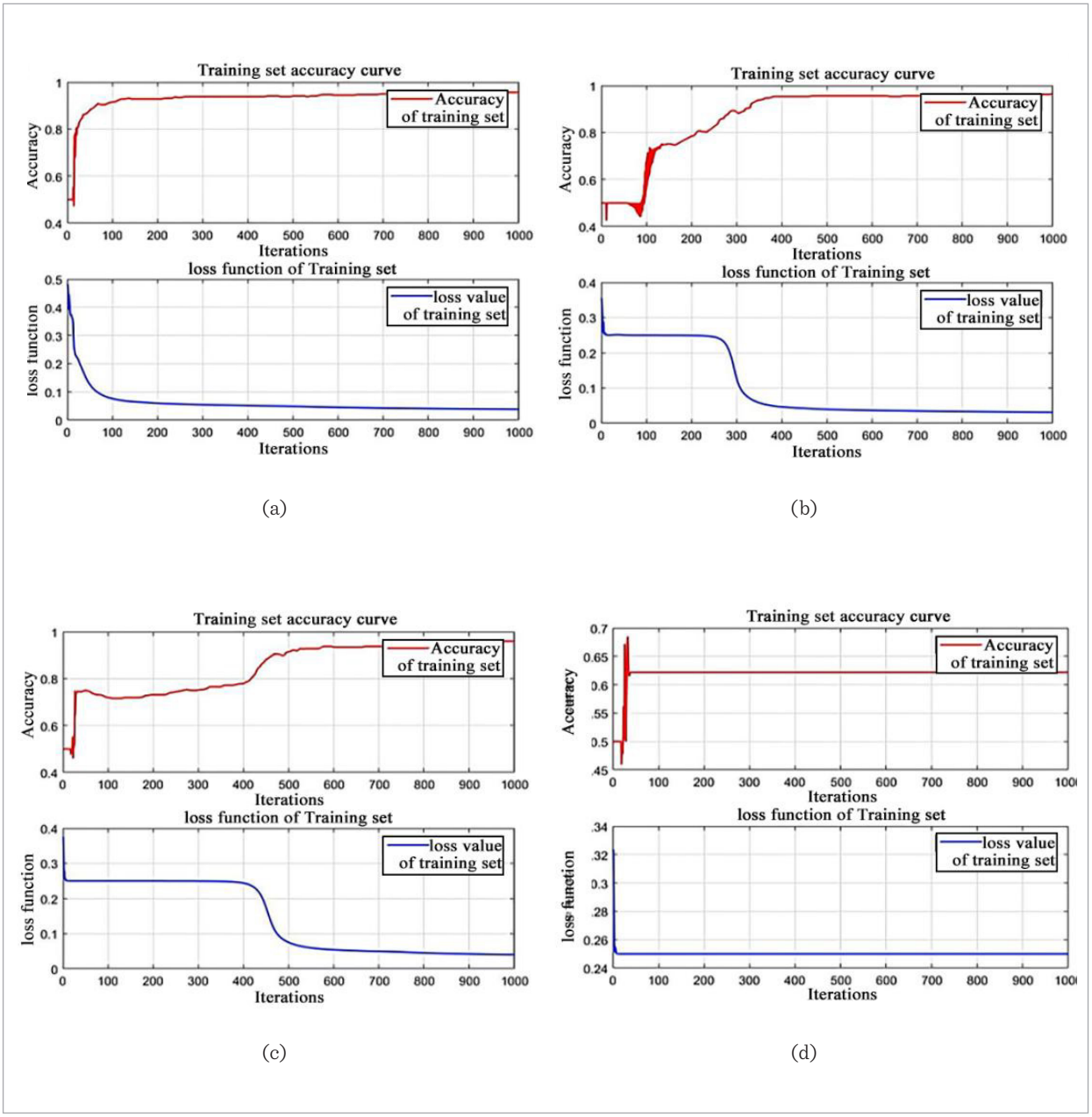

Figure 13

Effect of different reverse adjustment learning rates on the training process of the DBN with a 3-layer of Boltzmann machine and a prelearning rate of 0.007: (a) Training results with reverse adjustment learning rates of 2; (b) Training results with reverse adjustment learning rates of 1.5; (c) Training results with reverse adjustment learning rates of 2.5; (d) Training results with reverse adjustment learning rates of 3.0

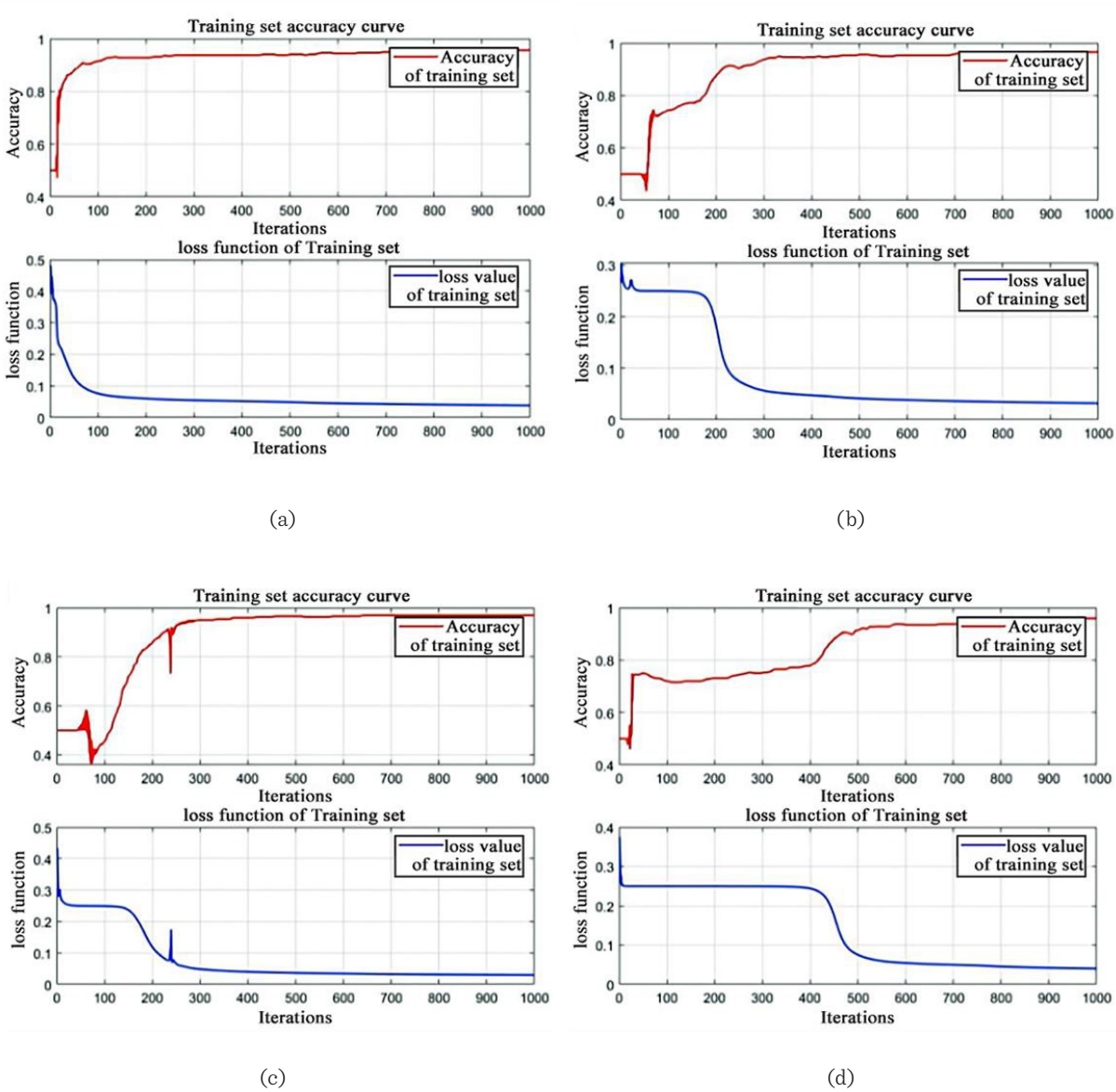

Table 2
Main parameters of the DBN

Three layers RBM	First layer	Second layer	Third layer
Number of neurons	44	30	30
Activation function		Sigmoid	
Pretraining times		1000	
Pretraining learning rate		0.007	
Number of reverse fine-tuning times		2000	
Reverse fine-tuning learning rate		2.0	

Figure 14
DBN training process

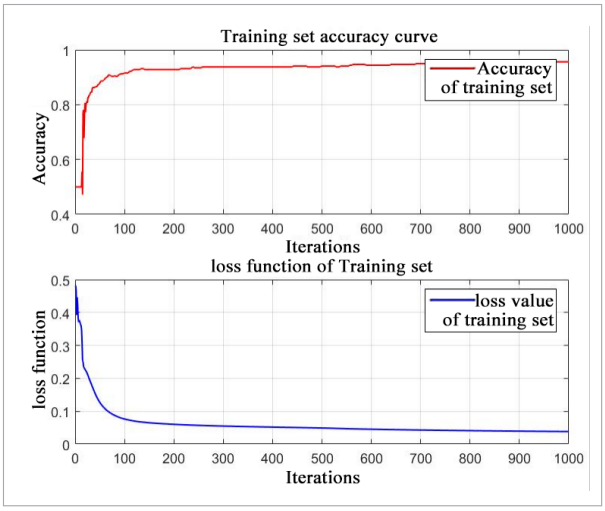

Figure 15
Confusion matrix of DBN training

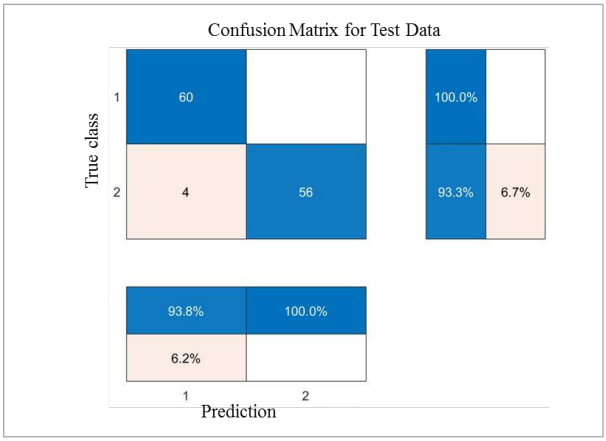

Figure 16
Training results for the experimental subjects

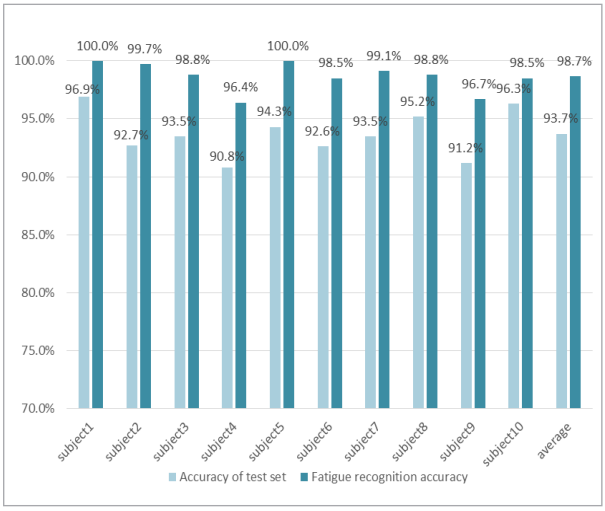

cal signals collected from an additional 9 participants into the model for training. The results are presented in Figure 16.

The results indicate that the model demonstrates excellent performance on the training data from the 10 participants, with an average test set accuracy of 93.2%. Notably, the fatigue state discrimination achieves an outstanding average accuracy of 98.8%. These results validate that the model exhibits high accuracy, generalizability, and robustness in discriminating driver states; in particular, the near-perfect discrimination accuracy for fatigued states is noteworthy.

6. Discussion

To further validate the accuracy of the model proposed in this paper, we established other driver fatigue state discrimination models, such as ICEEMDAN-BP and ICEEMDAN-DBN, for comparison with various denoising and classification algorithms. The obtained results are subsequently compared with those of the ICEEMDAN-WT-DBN model proposed in this study. The results are shown in Table 3.

By comparing the accuracy results of the six fatigue state discrimination models, it is evident that the

Table 3
Comparison of the discrimination accuracy among the three models

Training model	ICEEMDAN-WT-DBN	DBN	WT-DBN	ICEEMDAN-WT-BP	SVM	KNN
Accuracy/%	93.7	88.2	90.8	83.2	76.5	72.6

proposed ICEEMDAN-WT-DBN model achieves the highest discrimination accuracy. The accuracy of DBN training with raw data input without denoising is lower than that after denoising, indicating the significant impact of noise on the training accuracy. Moreover, WT-DBN, which relies solely on the wavelet threshold for denoising multimodal physiological signals, exhibits slightly lower accuracy than does the ICEEMDAN-WT-DBN model, suggesting its inferior ability to eliminate noise. Conversely, ICEEMDAN-WT-BP achieves a classification accuracy of only 82.2%, along with a slow convergence speed during runtime and susceptibility to local optima. Due to the limited ability of traditional machine learning classification algorithms to capture latent features within data, the accuracies achieved by SVM and KNN methods fall below 80%.

In the past, driver fatigue was primarily assessed based on vehicle driving conditions and driver facial expressions, which have certain limitations. Additionally, previous studies analysing the effects of multiple physiological signals and their combined applications are limited and have not yielded consistent conclusions. Building upon prior research, this study used a multimodal approach to analyse physiological signals to improve the assessment of driver fatigue.

In the past, studies on signal denoising have primarily concentrated on techniques such as wavelet threshold denoising. However, effectively removing noise signals with significant disturbances is challenging. To address this issue, this paper proposes a combination of the ICEEMDAN algorithm and wavelet threshold denoising method, which not only reduces noise in the signal but also enhances the signal recovery quality. The ICEEMDAN algorithm achieves fine multiscale decomposition to divide the signal into smoother and rougher parts while eliminating redundant components. On the other hand, wavelet threshold denoising determines thresholds based on subband variances to filter out high-frequency noise with lower energy while preserving useful information within the signal. The experimental results demonstrate that this approach is capable of filtering sharp noise signals as well as mitigating disturbances caused by subject activities.

In previous studies, traditional classifiers such as the support vector machine (SVM) and K nearest neighbour (KNN) algorithms have been used for classifying labelled datasets. However, these algorithms rely heavily on manual feature extraction, leading to suboptimal classification performance when dealing with data that possess ambiguous initial features such as multimodal physiological signals. In this study, we extract multidomain features from denoised EEG and EMG signals and use them as inputs for a DBN. By fully leveraging the deep feature extraction capability of the DBN, we construct the ICEEMDAN-WT-DBN fatigue state discrimination model, which reduces the computational complexity while improving the training and prediction efficiency. To determine appropriate model parameters, we use the grey wolf optimization algorithm to optimize the key DBN parameters. This approach eliminates the need for manually setting deep neural network parameters and further enhances the accuracy and robustness during model training.

7. Conclusion

In this paper, the method of combining ICEEMDAN and the wavelet threshold was used to denoise EMG signals. Then, multidomain feature extraction of the EEG and EMG signals was carried out. Finally, the features were input into the DBN for fatigue state discrimination. The main conclusions are as follows:

1 The present study proposes a novel denoising approach that combines the ICEEMDAN-WT method with physiological signal processing. Specifically, the ICEEMDAN algorithm is employed to decompose signals into multiple IMFs and effec-

tively eliminate redundant components through fine multiscale decomposition. Additionally, the WT is utilized to determine an adaptive threshold based on the variance of each subband, thereby filtering out high-frequency noise signals with minimal energy while preserving essential information to a significant extent. By integrating these two techniques, this study achieves remarkable denoising outcomes by not only eliminating high-frequency noise but also mitigating low-frequency disturbance signals.

2 The temporal domain, frequency domain, and nonlinear features of the denoised multimodal physiological signals are manually extracted in this study. A dataset is established with these manual features and input into a DBN for deep feature extraction. This approach reduces the data complexity while enhancing the real-time performance and robustness of the subsequent fatigue discrimination model.

3 The ICEEMDAN-WT-DBN fatigue driving discrimination model utilizes ICEEMDAN-WT for denoising the original signal and employs the grey wolf optimization algorithm to optimize the parameters of the DBN, thereby effectively enhancing the performance of the DBN. A comparative analysis with other fatigue discrimination models, including the DBN, WT-DBN, ICEEMDAN-WT-BP, SVM, and KNN models established in this study reveals that the proposed ICEEMDAN-WT-DBN model achieves a remarkable discrimination accuracy of 93.7%.

Funding

This research was funded by the Natural Science Foundation of China (62001312), the Joint Foundation of Liaoning Province (2023-MSLH-214), and Scientific Research Project of Department of Education of Liaoning Province (JYTMS20230315 and LJKZZ20220139).

Conflicts of Interest

The authors declare no conflicts of interest.

Data Sharing Agreement

The datasets used and/or analyzed during the current study are available from the corresponding author on reasonable request.

References

1. Aidman, E., Chadunowa, C., Johnson, K., Reece, J. Real-Time Driver Drowsiness Feedback Improves Driver Alertness and Self-Reported Driving Performance. Accident Analysis and Prevention, 2015, 81, 8-13. https://doi.org/10.1016/j.aap.2015.03.041
2. Amodio, A., Ermidoro, M., Maggi, D., Formentin, S., Savaresi, S. M. Automatic Detection of Driver Impairment Based on Pupillary Light Reflex. IEEE Transactions on Intelligent Transportation Systems, 2019, 20(8), 3038-3048. https://doi.org/10.1109/TITS.2018.2871262
3. Arefnezhad, S., Samiee, S., Eichberger, A., Fruhwirth, M., Kaufmann, C., Klotz, E. Applying Deep Neural Networks for Multi-Level Classification of Driver Drowsiness Using Vehicle-Based Measures. Expert Systems with Application, 2020, 162, 113771-113778. https://doi.org/10.1016/j.eswa.2020.113778
4. Barwick, F., Arnett, P., Slobounov, S. EEG Correlates of Fatigue During Administration of a Neuropsychological Test Battery. Clinical Neurophysiology, 2012, 123, 278-284. https://doi.org/10.1016/j.clinph.2011.06.027
5. Cai, J., Li, M., Zhao, C. Analysis of Driving Fatigue Detection Based on Combination Entropy Feature of EEG Signal. Electronic Test, 2022, 36, 43-47. https://doi.org/10.16265/j.cnki.issn1003-3033.2018.04.003
6. Chen, J., Wang, H., Wang, Q., Hua, C., Liu, C. Research on Fatigue Driving State Based on EEG Signals. Automotive Engineering, 2018, 40, 515-520. https://doi.org/10.19562/j.chinasae.qcgc.2018.05.003
7. Colominas, M. A., Schlotthauer, G., Torres, M. E. Improved Complete Ensemble EMD: A Suitable Tool for Biomedical Signal Processing. Biomedical Signal Processing and Control, 2014, 14, 19-29. https://doi.org/10.1016/j.bspc.2014.06.009
8. Dong, Y., Wang, L., Zhang, N., Chen, J. Analysis and Study of Surface EMG Signal Denoising Based on Combination of Variational Mode Decomposition and Wavelet Threshold. Journal of Shenyang Institute of Technology (Natural Science Edition), 2023, 19, 79-84. https://doi.org/10.13888/j.cnki.jsie(ns).2023.02.014
9. Feng, W., Cao, Y., Li, X., Hu, W. Face Fatigue Detection Based on Improved Deep Convolutional Neural Net-

work. Science Technology and Engineering, 2020, 20, 5680-5687. https://doi.org/10.1142/s0218001416601107

10. Forsmana, M., Vila, B., Shortc, R. A., Mottd, C. G., Dongena, P. A. Efficient Driver Drowsiness Detection at Moderate Levels of Drowsiness. Accident Analysis and Prevention, 2013, 50, 341-350. https://doi.org/10.1016/j.aap.2012.05.005
11. Glavic, D., Mladenovic, M., Stevanovic, A., Tubic, V., Milenkovic, M., Vidas, M. Contribution to Accident Prediction Models Development for Rural Two-Lane Roads in Serbia. Promet-Traffic & Transportation, 2016, 28(4), 415-424. https://doi.org/10.7307/ptt.v28i4.1908
12. Guan, Y., Tong, P., Feng, Z. Characterization of Fault Current Signal of Planetary Gearbox Based on ICEEMDAN Method and Frequency Demodulation. Journal of Vibration and Shock, 2019, 38, 41-47. https://doi.org/10.13465/j.cnki.jvs.2019.24.006
13. Jin, L. Research on Fatigue Driving Based on ECG Signals. Master, Chongqing University, Chongqing, 2017.
14. Lei, L., Feng, J., Zhao, Y., Yao, T., Hu, G. Design of Police Headband Based on EEG Signal Fatigue Driving. Computer Knowledge and Technology, 2019, 15, 204-207. https://doi.org/10.14004/j.cnki.ckt.2019.3487
15. Luo, H., Qiu, T., Liu, C., Huang, P. Research on Fatigue Driving Detection Using Forehead EEG Based on Adaptive Multi-Scale Entropy. Biomedical Signal Processing and Control, 2019, 51, 50-58. https://doi.org/10.1016/j.bspc.2019.02.005
16. Mahmoodi, M., Nahvi, A. Driver Drowsiness Detection Based on Classification of Surface Electromyography Features in a Driving Simulator. Proceedings of the Institution of Mechanical Engineers, Part H. Journal of Engineering in Medicine, 2019, 233, 395-406. https://doi.org/10.1177/0954411919831313
17. Nemcova, A., Seitl, M., Dominik, T., Semela, M., Sucha, M., Kolar, R., Svozilova, V., Bucsuhazy, K., Smisek, R., Mezl, M., Hesko, B., Belak, M., Bilik, M., Maxera, P. Multimodal Features for Detection of Driver Stress and Fatigue: Review. IEEE Transactions on Intelligent Transportation Systems, 2021, 22, 3214-3233. https://doi.org/10.1109/TITS.2020.2977762
18. Savas, B. K., Becerikli1, Y. Behavior-Based Driver Fatigue Detection System with Deep Belief Network. Neural Computing and Applications, 2022, 34, 14053-14065. https://doi.org/10.1007/s00521-022-07141-4
19. Sudha, K., Kumar, N., Tharani, K., Anand, A. Real-Time Driver Fatigue Surveillance System Using Machine Learning. Journal of Information and Optimization Sciences, 2022, 43, 239-244. https://doi.org/10.1080/02522667.2022.2044002
20. Wang, F., Wu, S., Ping, J., Xu, Z., Chu, H. EEG Driving Fatigue Detection With PDC-Based Brain Functional Network. IEEE Sensors Journal, 2021, 21, 10811-10823. https://doi.org/10.1109/JSEN.2021.3058658
21. Wang, H., Dragomir, A., Abbasi, N. I., Li, J., Thakor, N., Bezerianos, A. A Novel Real-Time Driving Fatigue Detection System Based on Wireless Dry EEG. Cognitive Neurodynamics, 2018, 12, 365-376. https://doi.org/10.1007/s11571-018-9481-5
22. Wang, L., Fu, R., Zhang, C., Yin, X., Hua, C., Wang, H. Research on Driving Fatigue Based on Approximate Entropy of Wireless Body Area Network and Composite Physiological Signals. Chinese Journal of Biomedical Engineering, 2017, 36(5), 543-549. https://doi.org/10.3969/j.issn.0258-8021.2017.05.005
23. Wang, L., Luo, X., Jiang, X., Wang, H. Detection on Driver Fatigue Based on Biomechanics and EMG of Cervical and Lumbar Muscles. Automotive Engineering, 2017, 39, 955-960. https://doi.org/10.19562/j.chinasae.qcgc.2017.08.016
24. Wang, X. S., Xu, C. Driver Drowsiness Detection Based on Non-Intrusive Metrics Considering Individual Specifics. Accident Analysis and Prevention, 2016, 95, 350-357. https://doi.org/10.1016/j.aap.2015.09.002
25. Wu, S., Gao, L., Wang, L. Detecting Driving Fatigue Based on Electroencephalogram. Transactions of Beijing Institute of Technology, 2009, 29, 1072-1075. https://doi.org/10.15918/j.tbit1001-0645.2009.12.013
26. Xi, X., Wu, H., Luo, Z. Surface EMG Signal Noise Cancellation Method Based on EMD Autocorrelation. Chinese Journal of Scientific Instrument, 2014, 35, 2494-2500. https://doi.org/10.19650/j.cnki.cjsi.2014.11.011
27. Xie, H., Zhou, X., Xia, B., Yang, W., Yao, N. Research on EEG Signal Feature Selection Algorithm and Support Vector Machine Model in Fatigue Driving Recognition. Chinese Journal of Biomedical Engineering, 2014, 33, 482-486. https://doi.org/10.3969/j.issn.0258-8021.2014.04.013
28. Ye, X. Alertness Analysis Based on EEG Signals in Simulated Driving Environment. Master's Thesis, Northeastern University, Shenyang, 2017.
29. Zhang, B., Chang, W., Li, X. Fatigue Driving Detection Based on Spatio-Temporal EEG Features and Parallel Neural Network. Journal of Transportation Systems Engineering and Information Technology, 2023, 23, 315-325. https://doi.org/10.16097/j.cnki.1009-6744.2023.02.033